Accumulating regions of winding periodic orbits in optically driven lasers

Bernd Krauskopf [a] and Sebastian Wieczorek [b]

[a] *Engineering Mathematics, University of Bristol, Bristol BS8 1TR, UK*

[b] *Physics and Astronomy, Vrije Universiteit Amsterdam, De Boelelaan 1081, 1081 HV Amsterdam, The Netherlands*

University of Bristol Applied Nonlinear Mathematics Preprint 2001.21

Abstract

We investigate the route to locking in class B lasers subject to optically injected light for injection strengths and detunings near a codimension-two saddle-node Hopf point. This is the parameter region where the Adler approximation is not valid and where Yeung and Strogatz recently reported a self-similar cascade of periodic orbits in the case of a solid-state laser. We explain this cascade as an accumulation of large regions bounded by saddle-node bifurcations of periodic orbits, but also containing further bifurcations, such as period doubling, torus bifurcations and small pockets of chaos. In the vicinity of the simultaneous saddle-node and Hopf bifurcations, successive periodic orbits wind more and more near the point in phase space where the saddle-node bifurcation is about to occur. This leads to a self-similar period-adding cascade.

By varying the linewidth enhancement parameter α from zero, the case of a solid state or CO_2 laser, to values larger than one, the case of semiconductor lasers, we show how the accumulating regions of winding periodic orbits change rapidly. This explains why the period-adding cascade has not been found in injected semiconductor lasers. Moreover, we are able to identify certain regions with complex dynamics in injected semiconductor lasers as 'remains' of the accumulating regions.

Key words: Lasers with optical injection, bifurcation diagrams, transition to locking
PACS: 42.50.Ne, 42.55.Px, 05.45.+b

1 Introduction

In this paper we are concerned with a physically and technologically important example of a periodically forced nonlinear oscillator: a laser subject to external

optical input with constant amplitude K and detuning ω (with respect to the frequency of the free running laser). One also speaks of an (optically) injected laser. Physically, the external light is produced by a second laser, also called the master laser, and it is sent into the first (or slave) laser via one of its partially reflective mirrors.

Optical injection was originally used to improve the optical properties of a given laser, in particular its spectral properties. Applications range from injection locking, frequency stabilization to line-width reduction and chirp reduction [1–5]. However, lasers, and in particular semiconductor lasers, subject to optical injection are also known to produce a large variety of dynamical behavior including complex and chaotic dynamics [6–39]; see also the surveys [40–42]. Originally, chaotic behavior of laser systems was seen as a nuisance to be engineered away, but more recently it was suggested [13] and studied [43] for chaotic communication schemes.

Apart from these more technology driven considerations, injected lasers are fascinating from a fundamental point of view, because they constitute the simplest laser system with complicated dynamics. For the important class B lasers, the system is described well by a set of three autonomous ordinary dimensional equations, the *single-mode rate equations* for the complex electric field E and the population inversion (the carriers) n. The control parameters are the injection strength K and the detuning ω (from the free-running laser) of the injected light. The single-mode rate equations are introduced in Section 2 and they are valid for solid-state, CO_2 and semiconductor lasers, or other class B lasers. These lasers are distinguished by the value of the so-called linewidth enhancement factor α: for solid-state and CO_2 lasers α is practically zero, while semiconductor lasers are characterised by a value of α in a typical range of about 1 to 10. The 'single-mode' in the name of the equations already indicates that the basic assumption is that the laser lases at a single frequency throughout, which is the case, for example, for distributed feedback (DFB) laser [37,44]. However, even for Fabry-Perrot lasers (the simplest type of lasers where a lasing material is located between two mirrors) that may show 'hopping' between different laser modes, the assumption of single mode operation turned out to be valied for large regions of operation [22].

The first goal of this paper is to present and explain a complicated structure for $\alpha = 0$ of accumulating regions in the (K, ω)-plane where winding periodic orbits exist with an increasing number of small loops; see already Figure 3. More specifically, the accumulating regions appear near a codimension-two saddle-node Hopf (SN-Hopf) bifurcation [45,46] on the boundary of the locking region. The saddle-node bifurcation takes place on a periodic orbit, leading to a global reinjection mechanism. We speak of a SN-Hopf bifurcation with global reinjection.

The direct motivation for our study for $\alpha = 0$ is the recent paper by Yeung and Strogatz [26], where a rate equation model of a solid-state laser (equivalent to (1) for $\alpha = 0$) is studied. Injection is viewed as unidirectional coupling and as a step towards understanding two bidirectionally coupled lasers [47]. The paper reports on a new route to locking in an intermediate regime between locking via a saddle-node bifurcation and locking via Hopf bifurcation. This route to locking involves cascades of winding periodic orbits, interspersed with more complicated dynamics. Yeung and Strogatz encouraged more research into this phenomenon [26, p.4433]: "From a theoretical perspective, the most interesting open question concerns the mathematical mechanism underlying the self-similar cascade of bifurcations." We identify this new route to locking here as a period-adding sequence that occurs along (suitable) one-parameter paths through the accumulating regions of winding periodic orbits.

However, the problem of periodic orbits with increasing numbers of small windings has received quite some attention in different types of optically driven lasers before, in both theoretical models and real experiments. In 1985 Brun et al. [48] presented experimental time series as well as computer simulations of periodic orbits with increasing number of small wiggles when increasing the amount of the light injected into a ruby nuclear-magnetic-resonance laser. In the same year Tredicce [49] predicted the similar phenomenon of large pulses (corresponding to large loops) separated by different numbers of small amplitude relaxation oscillations (small wiggles) for a CO_2 laser. His results were experimentally confirmed by Boulnois [50] in an experiment with a CO_2 laser. In 1988, Lauterborn and Eick [51] studied a route to locking in an injected laser with saturable absorber and reported the existence of periodic solutions with increasing windings. They produced images of the associated cascade of winding periodic orbits and identified it as a period-adding cascade. The windows of more complicated dynamics contain further windows of locking regions, which are organised by the Frechet numbers [51, p. 1092].

Our second goal is to explore what happens to the structure of accumulating regions of winding periodic orbits when α is increased towards values typical for semiconductor lasers. Our direct motivation is the fact that the period-adding route to locking has never been found in semiconductor lasers, both theoretically and in experiments. We show here that the structure breaks up already for very small values of α, explaining that it was found only for CO_2 and solid-state lasers. On the other hand, we can trace certain regions in parameter space with complicated dynamics for lasers with $\alpha > 0$ back to this structure. This includes a structure of resonance tongues along a torus bifurcation curve near the SN-Hopf point for $0 < \alpha < 1$, that was recently studied in detail by Mayol et al. [36]. In their paper the authors conjecture that this structure may be connected to the phenomenon described in [26], and our results show that this is indeed the case. The main difference is that the resonance tongues studied in [36] do not give rise to attracting winding

orbits, so that there is no period-adding cascade. Finally, we are able to make a connection to complicated bifurcation structures for the case of an injected semiconductor laser (with $\alpha > 1$), which we studied extensively in earlier work [29–31,33,34].

The paper is organised as follows. In section 2 we introduce the rate equations of a class B laser with injection. In section 3 we describe the regions of winding periodic orbits and reveal other bifurcation structures, such as pockets of chaotic dynamics. Section 4 is concerned with what happens to the bifurcation diagram in the (K, ω)-plane when α becomes positive and reaches values up to $\alpha = 2$. In section 5 we draw conclusions and point out directions for future studies.

2 Class B laser with optical injection

In a semiclassical approach to laser theory the laser medium is described by the quantum-mechanical Schrödinger equation and the light propagation is governed by the classical Maxwell equations. This works remarkably well for most types of lasers [52]. It leads to the rate equations, the so-called Maxwell-Bloch equations, for the slowly varying complex electric field E in the laser cavity, the polarization P of the active medium, and the population inversion n (number of electrons in the excited state). Depending on the magnitude of the decay times for these dynamical variables Arecchi et al. [53] distinguished between different classes of lasers. Class C lasers have similar decay rates for the electric field, polarization and population inversion and need to be described by the full set of Maxwell-Bloch equations. In class B lasers, which are the subject of our studies, the polarization decays on a much shorter time scale than E and N and, hence, becomes a follower of E that can be adiabatically eliminated. Solid-state, CO_2 and semiconductor lasers are all class B lasers.

After suitable scaling, the rate equations for a class B laser with optical injection take the form

$$\begin{aligned} \dot{E} &= K + \left(\frac{1}{2}(1+i\alpha)n - i\omega\right) E \\ \dot{n} &= -2\Gamma n - (1+2Bn)(|E|^2 - 1) \ , \end{aligned} \tag{1}$$

where $E = E_x + iE_y$ is the ecomplex electric field and n is the population inversion. See [29] for more details on the derivation of these dimensionless equations, and for information on how to relate the scaled quantities to physical laser parameters. The two key parameters are the injected field amplitude K and the detuning ω, and both can easily be adjusted in an experiment.

The other parameters specify material properties of the laser, namely B is the rescaled cavity life time of photons in the laser cavity and Γ is the rescaled damping rate of the so-called relaxation oscillations, a periodic exchange of energy between the electric field E and the carriers N. Throughout this paper we use the realistic values $B = 0.015$ and $\Gamma = 0.035$ [29].

The third material constant, α, is very important. It is a measure for the self-phase modulation of the laser, that is, for the coupling between the phase and the amplitude of the electric field E and is called the *linewidth enhancement factor*. The value of α is what distinguishes different types of class B lasers. For solid-state and CO_2 lasers α is practically zero. On the other hand, semiconductor lasers have typical values of α larger than one. This means that changing the output power of a semiconductor laser heavily influences its lasing frequency. This effect is also called chirping, and it is due to a change of the refractive index of the semiconductor material with the amount of light in the cavity.

The single-mode rate equations have been studied (in forms equivalent to (1); see also [38,40,41]) by reducing them to two-dimensional averaged equations, e.g. in [14,18,24,25,38], and by considering certain limits, e.g. in [20,27,28]. The study of the full three-dimensional rate equations started with bifurcation studies using numerical integration, e.g. in [17,21,32], but recently also made use of bifurcation theory methods such as the direct continuation of bifurcation curves, e.g. in [23,29,30,34,36,39]. All these studies showed very good agreement with experiments, in particular, with experimental stability maps [15,22,37].

In this paper we are concerned with the bifurcation diagram in the (K, ω)-plane for different fixed values of α of the three-dimensional system (1). (Note that B and Γ change only little for different lasers and remain fixed in this paper.) We first study the case $\alpha = 0$ of a solid-state or CO_2 laser, and then discuss what happens when α is increased to typical values of semiconductor lasers.

Saddle-node bifurcation curves were plotted using analytical expressions, while all other bifurcation curves were calculated with the continuation package AUTO [54]. For a particular laser, α stays fixed and the bifurcations are continued in the (K, ω)-plane resulting in a bifurcation diagram for this type of laser. We first computed the bifurcation diagram for $\alpha = 0$ and then followed the respective bifurcations to higher values of α, stopped at certain values $\alpha > 0$ and computed the respective bifurcation diagrams in the (K, ω)-plane for these values of α. In this manner, we followed the regions of winding periodic orbits that we found for $\alpha = 0$ to higher values of α all the way up to the case of an injected semiconductor laser. The associated phase portraits were computed with the package DsTool [55].

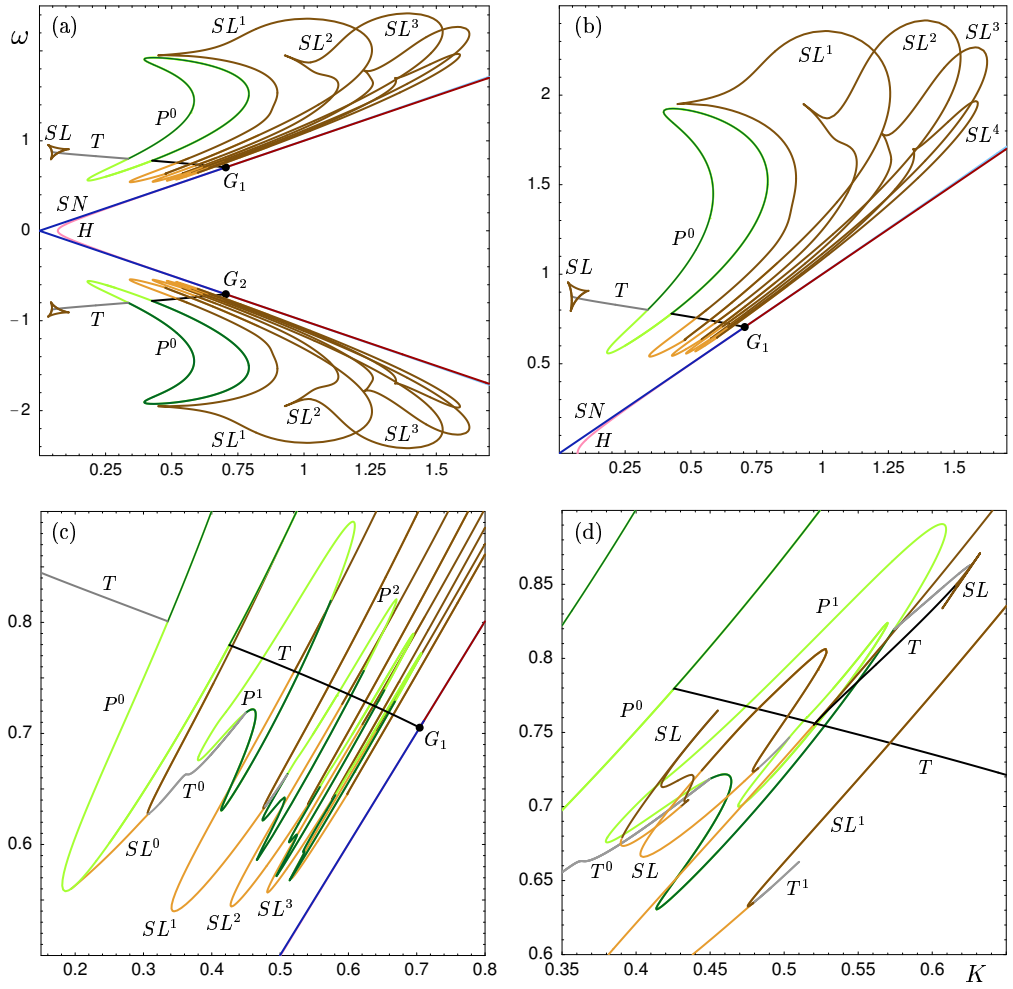

Fig. 1. Accumulating regions of winding periodic orbits for $\alpha = 0$ (top row) and their detailed structure near the point G_1 in two consecutive enlargements (bottom row).

3 The (K, ω)-plane for $\alpha = 0$

We now describe in detail the bifurcation curves and corresponding dynamics in phase space associated with the accumulation of large regions of winding periodic orbits near the codimension-two SN-Hopf points G_1 and G_2 for $\alpha = 0$. Figure 1 (a) shows an overview of the bifurcation diagram in the (K, ω)-plane for both positive and negative values of the detuning ω. Darker colors correspond to supercritical and lighter color to subcritical bifurcations. Notice that the bifurcation diagram of (1) is reflectionally symmetric for $\alpha = 0$ under the symmetry $(E, \omega) \to (E^*, -\omega)$. This is why for the remainder of this section we restrict to the case of positive ω shown in Figure 1 (b).

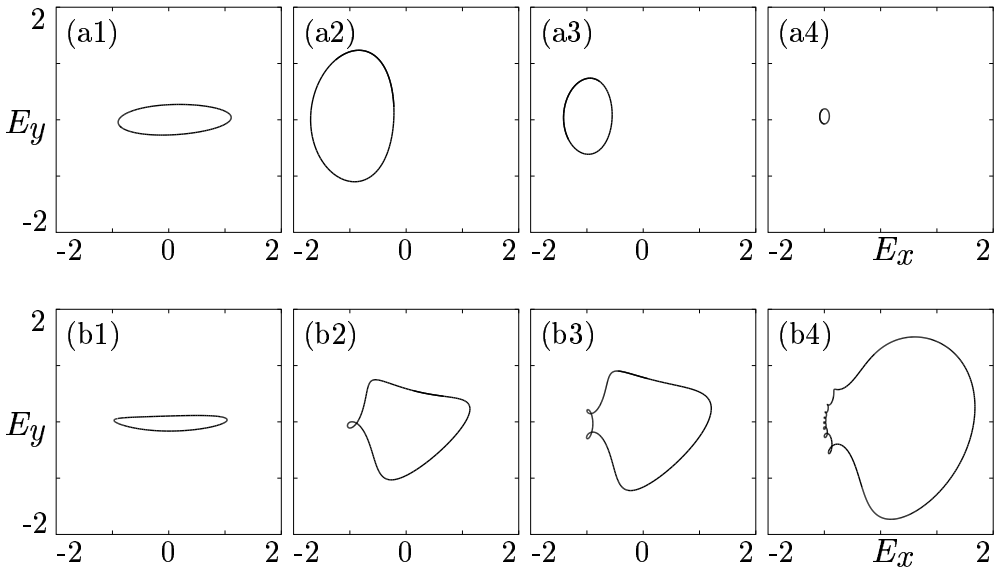

Fig. 2. Different locking mechanisms. Above the point G_1 locking occurs in a Hopf bifurcation (top row), and below G_1 and below the accumulating regions in Figure 1 it occurs in a saddle-node bifurcation on a periodic orbit (bottom row). In (a1) to (a4) $\omega = 0.8$ and K takes the values 0.05, 0.5, 0.7, and 0.795; in (b1) to (b4) $\omega = 0.5$ and K takes the values 0.05, 0.32, 0.396, and 0.48.

3.1 Entering the locking range

The saddle-node curve SN and the Hopf curve H are very close together and they touch at the two SN-Hopf bifurcation points G_1 and G_2, where they change from super- to subcritical. As a consequence, the locking range, where the laser locks to the input, is the cone-like region bounded by the supercritical part of H and the supercritical part of SN. In other words, when one starts with the solitary laser solution, the locking range is generally entered either via a Hopf bifurcation, for ω above G_1 (and below G_2), or via a saddle-node bifurcation, for positive ω well below G_1. This is illustrated in Figure 2 where in panels (a1)–(a4) we follow the running phase solution to the locking at the Hopf bifurcation, while panels (b1)–(b4) follow the running phase solution up to the locking at the saddle-node bifucation well below G_1 (below the end of the accumulating bifurvation curves). Notice that the saddle-node bifurcation takes place on a periodic orbit. On the way to locking the running phase solution develops an increasing number of windings close to where the equilibrium will appear in the saddle-node bifurcation. This is due to the fact that the laser operates close to the SN-Hopf point G_1 with a slow passage near a region with transverse spiralling.

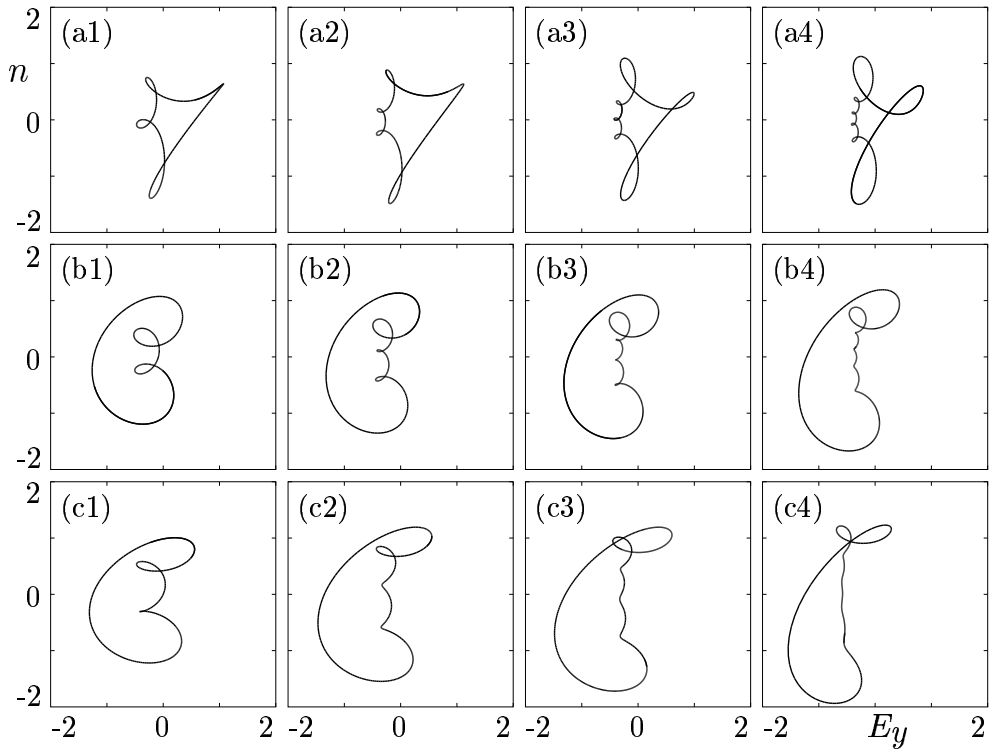

Fig. 3. Periodic orbits existing inside the first four large regions plotted for three different values of the detuning. In (a1) to (a4) $\omega = 0.8$ and K takes the values 0.588, 0.67, 0.71, and 0.735; in (b1) to (b4) $\omega = 1.3$ and K takes the values 0.99, 1.095, 1,15, and 1,181; in (c1) to (c4) $\omega = 1.8$ and K takes the values 1.2, 1.38, 1.48, and 1.529.

If one follows the running phase solution at the intermediate range of ω near and below G_1 then one encounters a period-adding sequence as observed in [26]; see also [51]. How this can be explained is quite intricate, as we will see in the remainder of this section.

3.2 Self-similar structure of bifurcations

The closed curves of saddle-node bifurcations of limit cycles SL^j for $j = 1, 2, \ldots$ in Figure 1 bound regions of attracting periodic orbits with an increasing number of windings. These regions accumulate on the saddle-node curve SN, but they also overlap for larger values of ω. In Figure 3 we show what these limit cycles look like for SL^1 to SL^4 for different values of the detuning, but all above the curve T. These periodic orbits always coexist with the running phase solution of the laser, which is the continuation of the solution of the free-running laser (for $K = 0$). Due to the overlap of the regions

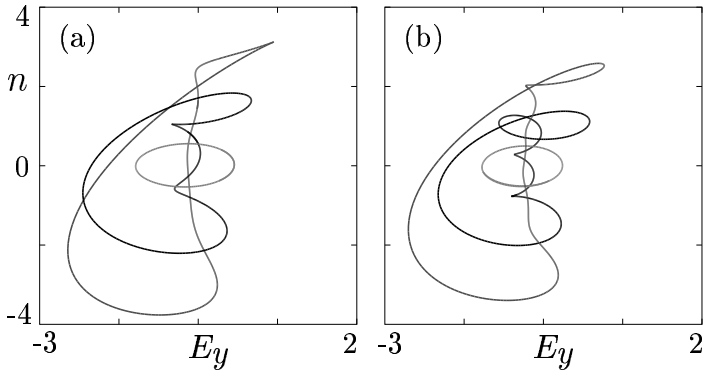

Fig. 4. Coexistence between the running phase solution and different winding periodic orbits where the large regions overlap; $\omega = 1.9$, and $K = 1.15$ (a) and 1.45 (b).

of their existence, several periodic orbits with different numbers of windings can coexist with the running phase solution, as is shown with two examples in Figure 4. This is why the route to locking, when one follows the running phase solution from $K = 0$ above T is always via the Hopf bifurcation at H.

Near G_1 the structure of the bifurcation diagram is very complicated, as is shown in the enlargements in Figure 1 (c) and (d). The curves SL^j change from super- to subcritical near the curve T in 1:1 resonances which results in the creation of new torus curves labeles T^j in Figure 1 (d). At the same time there are small bubbles of period-doubling curves P^j that change from super- to subcritical in 1:2 resonances, which are again associated with torus bifurcations. Furthermore, there are smaller and smaller regions bounded by new saddle-node bifurcations of limit cycles (denoted simply SL), which again change from super- to subcritical in resonances. They are associated with periodic orbits that make a number of large excursion so that they pass the phase space region of winding several times. The overall picture is that of a nested sequence of closed curves of period-doubling and saddle-node curves that are connected by torus bifurcation curves at codimension-two resonance points.

The closed curves S^j look like resonance tongues of locked orbits on an attracting torus, but in fact they are not. They bound regions with an attracting and a saddle-type periodic orbit with a given number of windings, but it is also possible to follow an orbit continuously from one such region to the next by following the orbit inside the first region to well below the curve T (where the SL^j are subcritical) and then into the next region. The limit cycle picks up one more winding along the way in a continuous fashion. However, when one keeps ω fixed near G_1 and sweeps K one encounters a complicated sequence of bifurcations.

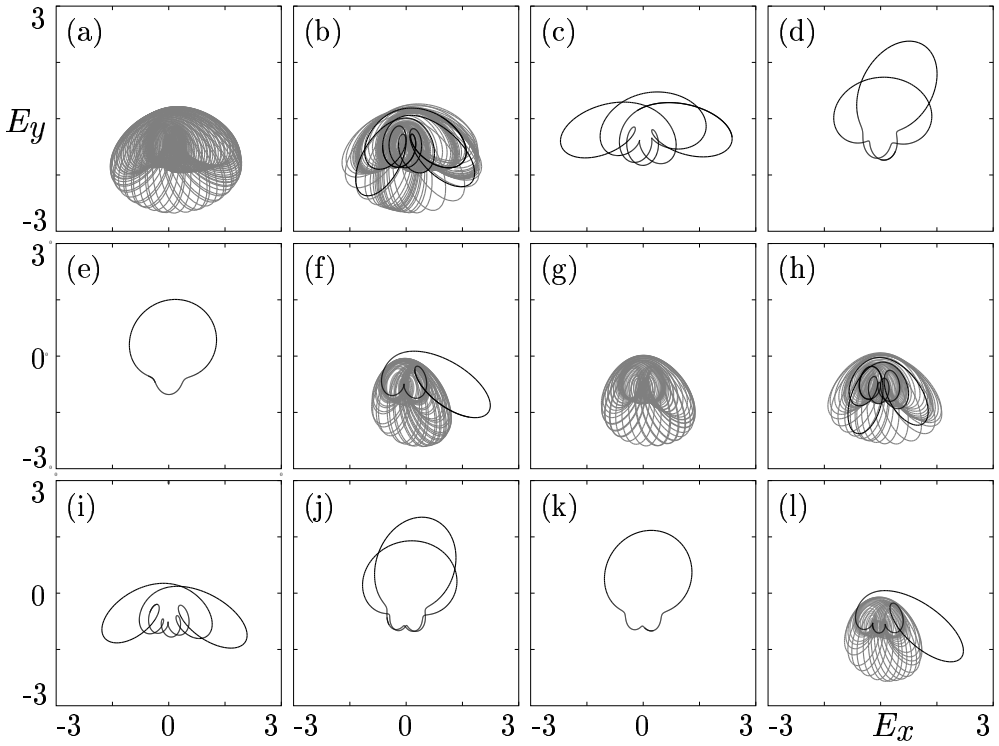

Fig. 5. The first two steps in the transiton to locking via the period-adding cascade; $\omega = 0.7$ and from (a) to (l) K takes the values 0.401, 0.40415, 0.415, 0.475, 0.49, 0.532, 0.54, 0.5468, 0.55, 0.573, 0.575, and 0.598.

3.3 Period-adding route to locking

This complicated arrangement of bifurcation curves is the explanation for the period-adding route to chaos that one finds near G_1 below the curve T. The first two steps of it are illustrated with phase portraits in Figure 5. Starting with a stable torus [Fig. 5 (a)] we cross SL (which has a characteristic spiky cusp) [Fig 1 (d)] and an attracting periodic orbit is born which coexists with the torus [Fig. 5 (b)]. The torus is then destroyed in a homoclinic bifurcation, involving the saddle-type periodic orbit also born along the same curve SL, as is explained in Section 3.4. Note that for slightly different detunings another small curve SL can be crossed and the torus disappears in a homoclinic bifurcation with a periodic orbit with a different number of large excursions. In any case, as a result only the attracting periodic orbit is left [Fig. 5 (c)]. This periodic orbit undergoes a series of complicated bifurcations, including small pockets of chaotic dynamics; see Section 3.5 and Figure 8. Finally, a different attracting limit cycle remains [Fig. 5 (d)] which then period-undoubles along P^1 [Fig. 5 (e)]; compare Figure 1 (d). Then, the torus reappears via a homoclinic tangency bifurcation of the saddle orbit originating from SL^1 in a similar fashion as it was destroyed and coexists with the periodic orbit [Fig. 5

(f)]; see Section 3.4. The periodic orbit disappears along SL^1 and we are back to a situation with only an attracting torus [Fig. 5 (g)]. When K is increased further, we see in Figure 5 (g)–(l) a repetition of the transition we saw in Figure 5 (a)–(f). The difference is that the periodic orbits involved now, in particular the orbit accompanying the reappearence of the torus, are wound up by one more turn. This means that we are crossing a similar structure as before, but for the next region in the accumulation of bifurcation curves. When one plots points in a Poincaré section, one observes windows of periodic orbits with, successively, an extra point in the plot: a period adding cascade. These windows accumulate on the parameter value corresponding to the curve SN in Figure 1 (c).

3.4 Homoclinic break-up of tori

That the curves S^j are not associated to locked orbits on a torus can also be seen by the fact that the bifurcating attracting periodic orbits coexist with the torus; see Figure 5 (b) and (f). The torus then disappears by colliding with the bifurcating saddle-type periodic orbit, which happens via a first and a last homoclinic tangency of the stable and unstable manifolds of the saddle-type periodic orbit.

This process is illustrated in Figure 6 where we show what happens in the Poincaré section $\{n = 0\}$. First there is only the invariant torus, that is, an attracting invariant closed curve in the Poincaré section with a repellor inside it [Fig. 6 (a)]. The dynamics on the invariant curve appears to be quasiperiodic. This situation corresponds to that in Figure 5 (a) and (g). After the saddle-node bifurcation we see an attractor and a saddle periodic orbit [Fig. 6 (b)]. The number of intersections with this Poincaré section defines the number of windings, which is seven in this case. However, it can be different for different values of the detunig because another small curve SL can be crossed. We computed the stable and unstable manifolds of the saddle-points with the method in [56,57] under DsTool [55]. The stable manifolds (in blue) come from the central repellor, dividing the interior of the torus into the basins of the attractors and that of the torus. One branch on the unstable manifolds (in red) goes to the respective attractor and the other to the attracting invariant curve (the intersection of the torus with the section). This situation corresponds to that in Figure 5 (b) and (h). The invariant curve (or the torus) breaks up in a first tangency (which is not shown here) between the stable and unstable manifolds, and then there is a very small region with homoclinic tangle [Fig. 6 (c)]. As is well-known, there is chaotic dynamics associated with shift dynamics in the region with homoclinic tangle. After a last homoclinic tangency both branches of the unstable manifolds now go to attractors and the torus is gone [Fig. 6 (d)]. This situation corresponds to that in Figure 5 (c) and (i).

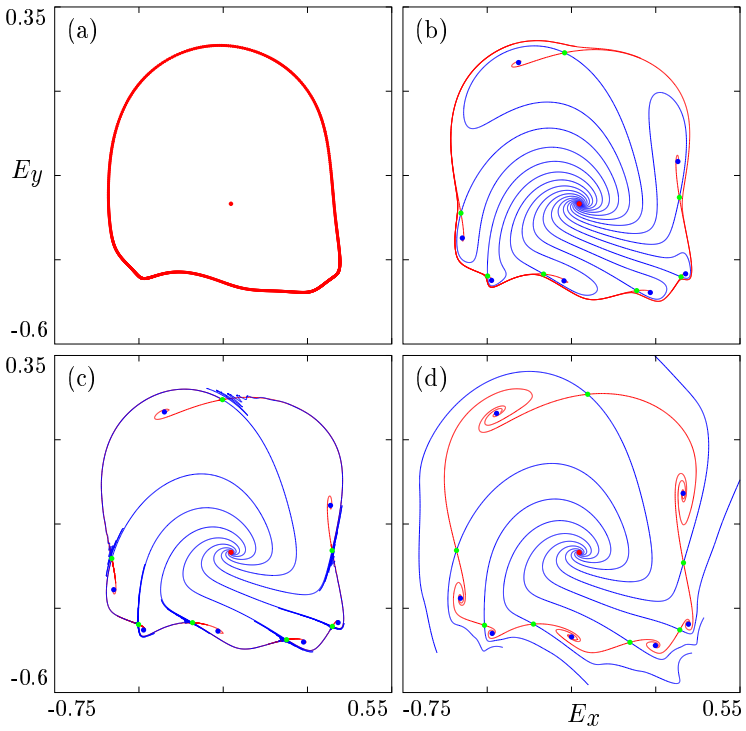

Fig. 6. Homoclinic tangencies are reponsible for the destruction of the torus appearing in the period adding cascade to locking, shown in the Poincaré section $\{n = 0\}$. The torus (a), then coexists with two periodic orbits born on SL (b), after a first homoclinic tangency there is homoclinic tangle between the stable (blue) and unstable (red) manifolds (c). After a last homoclinic tangencies the manifolds split (d); $\omega = 0.7$ and from (a) to (d) K takes the values 0.4, 0.404, 0.4042, and 0.405.

The reappearence of the torus [Fig. 5 (f) and (l)] is due to the reverse bifurcation scenario, when increasing K further. The only difference is that the emerging periodic orbits are now outside the torus, as is shown in Figure 7 where the periodic orbits intersect the chosen Poincaré section in three points. Just before the torus reappears [Fig. 7 (a)] both branches of the unstable manifold (in red) go to attracting periodic orbits (blue points). After a first homoclinic tangency, there is a homoclinc tangle [Fig. 7 (b)]. After a last homoclinc tangency the torus is created, and one branch of the unstable manifold goes to periodic orbit while the other accumulates on the attracting invariant curve corresponding to the torus [Fig. 7 (c)]. After the periodic orbits disappear when SL^1 is crossed, the torus is the only attractor [Fig. 7 (d)].

It is worth noting that during the period-adding cascade a torus is destroyed (or created) by 'colliding with' periodic orbits originating along saddle-node of limit cycle curves SL. When the main curves SL^j are crossed then the bifurcating periodic orbits make one big loop around the origin of the complex E-plane and j windings of wiggles near where the saddle-node appears. This leads to an increasing number of intersection points in the Poincaré section

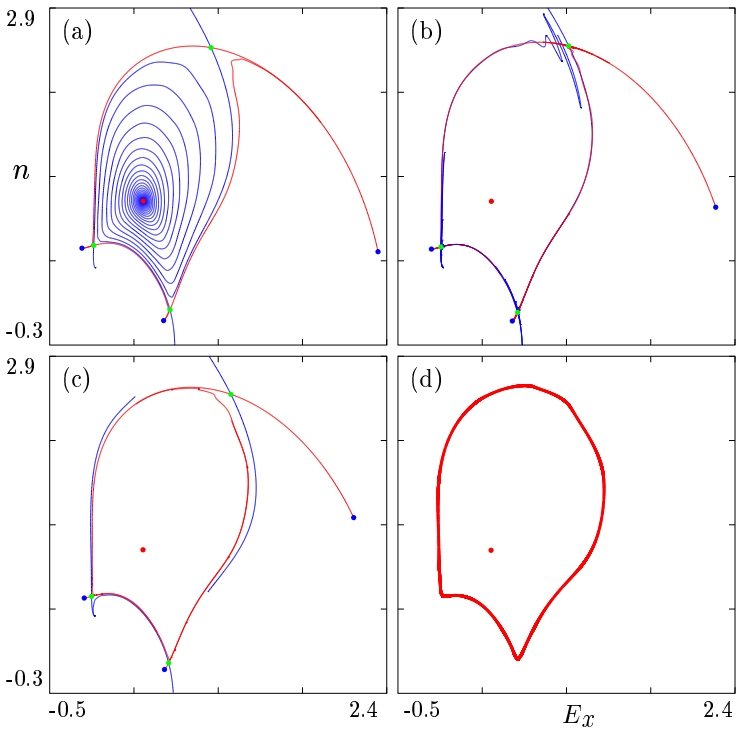

Fig. 7. The tori involved in the period-adding cascade reappear via homoclinic tangencies of winding saddle orbits, which exist in the large regions. The panels show attractors in the Poincaré section $\{E_y = -1\}$; $\omega = 0.69$ and from (a) to (d) K takes the values 0.522, 0.52283, 0.5235, and 0.525.

$\{n = 0\}$. When smaller curves SL are crossed the bifurcating periodic orbits make a number of big loops around the origin of the complex E-plane, with a certain number of windings along each of these big loops. There are more big loops the deeper one enters into the complicated bifurcation structure. When the number of big loops stays the same, but new windings appear, the period of the periodic orbit (of the vector field) does not change much, but the period of the corresponding periodic points of the Poincaré map does increase by one at each step. By taking a local Poincaré section far from where the saddle-node will appear, one can make sure that these periodic orbits lead only to a single intersection point for each big loop. Extra windings will then not be picked up as extra points in the Poincaré section since they appear far away from the section. This shows that the break-up of the tori in the homoclinic tangencies described above is not due to weak $p : q$ resonances, near which one would expect locking on the torus instead; see, for example, [46].

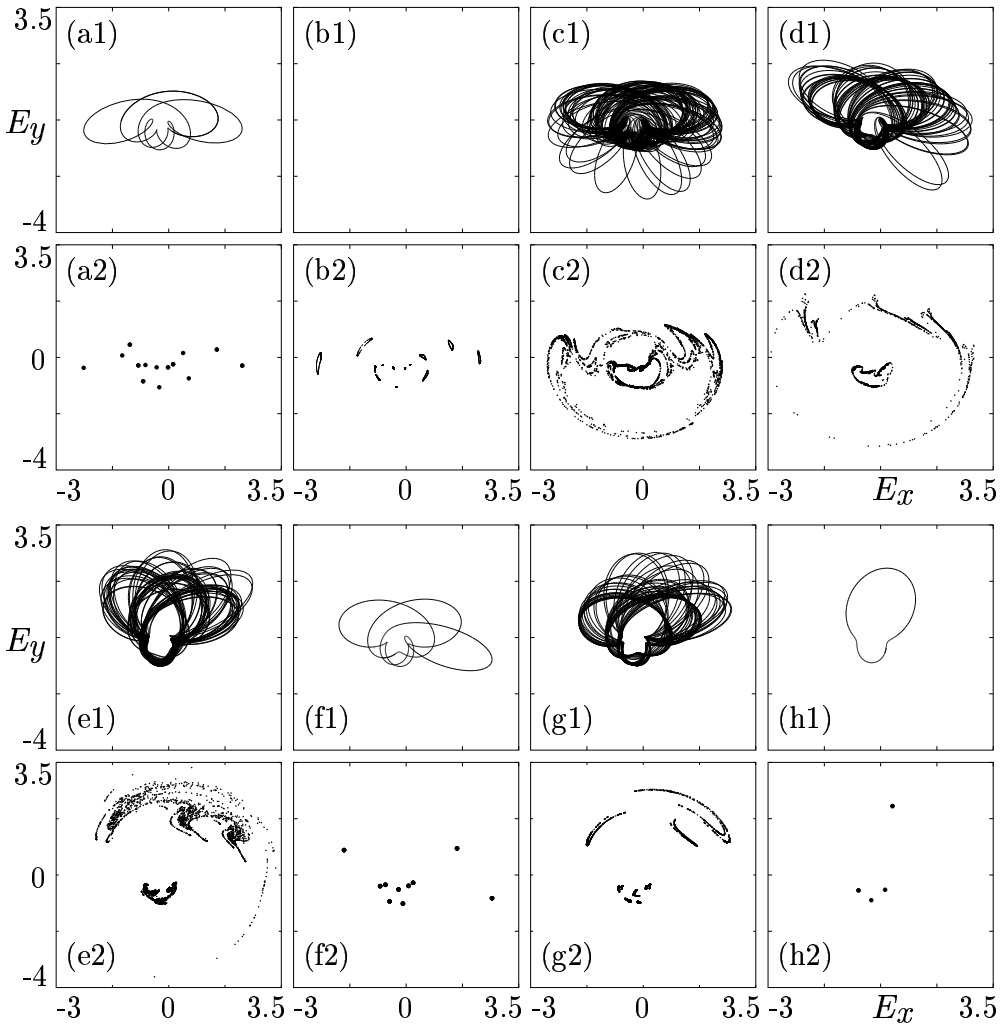

Fig. 8. Transition through regions of chaos. The upper rows show attractors projected onto the E-plane, while the bottom rows show their intersections with the Poincaré sections $\{n = 0\}$; $\omega = 0.7$. and from (a) to (h) K takes the values 0.415, 0.4173, 0.419, 0.422, 0.423, 0.43, 0.438, and 0.44.

3.5 Pockets of chaos

The transition between Figure 5 (c) and (d), and between Figure 5 (i) and (j), is not just a continuous deformation of the periodic orbit. In fact, many additional bifurcations are involved, as can already be surmised from the bifurcation curves that need to be crossed in Figure 1 (d). What actually happens is shown in Figure 8 by two panels for each parameter value, one showing the respective attractors of the vector field and the other their intersections with the Poincaré section $\{n = 0\}$. The chain of events contains pockets of chaos.

The attracting periodic orbit [Fig. 8 (a)] bifurcates into a torus [Fig. 8 (b)] which then breaks up into a chaotic attractor [Fig. 8 (c)]. It changes its shape as K is increased further [Fig. 8 (d) and (e)]. There is a region of locking to a period-three orbit [Fig. 8 (f)] and then the chaotic attractor develops a shape [Fig. 8 (g)] that is usually associated with a chaotic attractor arising from a period-doubling route to chaos. However, the chaotic attractor disappears suddenly in a boundary crisis [Fig. 8 (h)], it hits its basin and all trajectories 'leak' to the coexisting periodic orbit. This periodic orbit period-doubles and then we reach the situation in Figure 5 (d).

We remark that this transition appears to be globally the same for all steps in the period-adding cascade, with the difference being the number of windings of the participating periodic orbits.

4 The (K, ω)-plane for positive α

The period-adding cascade is a possible transition to locking when $\alpha = 0$, that is, for solid-state or CO_2 lasers. However, there are other types of lasers, most importantly, the widely used semiconductor lasers which have values of α in the range from about 2 to 5 (or even up to $\alpha = 10$). For semiconductor lasers a period-adding cascade has never been reported. The question arises what happens to the complicated structure in Figure 1 when α is increased from zero to the range one finds for semiconductor lasers.

We show now that the regions of winding periodic orbits start to disappear already for very small positive α. On the other hand, some of the regions we found, in particular, those bounded by the curves SL^i, survive and can be followed for increasing α. In this way, we can identify important regions associated with chaos in the (K, ω)-plane of semiconductor lasers as 'remainders' of the accumlating regions for $\alpha = 0$. Because increasing α from zero breaks the symmetry of the (K, ω)-plane, we consider the cases of positive and negative detuning separately.

4.1 Positive detuning

What happens to the (K, ω)-plane when α is varied is shown in Figure 9, where panel (a) repeats the (K, ω)-plane for $\alpha = 0$ and positive ω. Initially the bifurcation curves shown in the (K, ω)-plane do not change much for small values of α; see Figure 9 (b). This shows that for realistic lasers, for which α is small but never exactly zero, there is indeed a period-adding cascade to locking near the point G_1, as was reported in the literature [50,48,51,49].

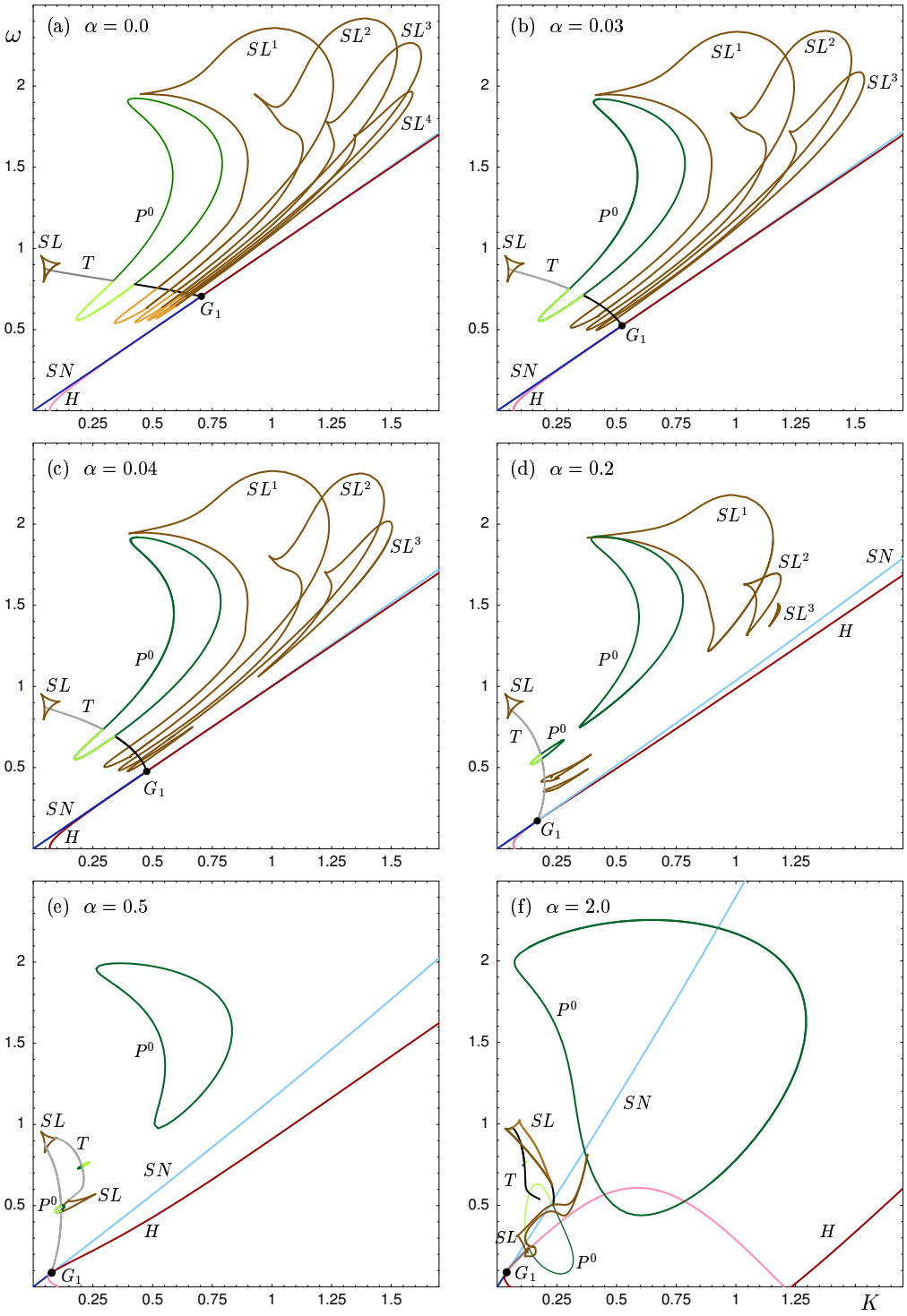

Fig. 9. Transition of the accumulating regions in the (K, ω)-plane for positive detunings ω with increasing α; from (a) to (f) α takes the values 0.0, 0.03, 0.04, 0.2, 0.5, and 2.0.

However, already for $\alpha = 0.04$ we see that the regions bounded by SL^i for larger i start to break apart into two regions, a small one near G_1 and a larger one for larger ω; see Figure 9 (c). Our computations indicate that this process starts for very large values of i as soon as $\alpha \neq 0$. The larger α becomes, the more regions break apart, and for $\alpha = 0.2$ all regions bounded by SL^i are affected, as is shown in Figure 9 (d). At the same time, the respective remaining regions shrink further and seem to disappear. Furthermore, for $\alpha = 0.2$ also the large region bounded by the period-doubling curve P^0 has split into two pieces. For even larger values of α, but $\alpha < 1$ we are left with two regions bounded by P^0, one large and the other tiny, and a structure of resonances along the torus curve T coming from G_1; see Figure 9 (e). An image of this structure for $\alpha = 0.5$ near G_1 can already be found in [29, Fig. 5], and it was recently analysed in detail in [36]. In answer to the discsussion in [36] we remark that this structure is not the transition to locking studied in [26], because the involved bifurcations do not lead to attracting periodic orbits.

It is well-known that the SN-Hopf point G_1 undergoes a change from type II to type III in the notation of [45] when α is changed through one; see [14,24]. From then on, the (K, ω)-plane has some features that are typical for semiconductor lasers. This is illustrated in Figure 9 (f) for $\alpha = 2$. Notice that the supercritical part of the Hopf curve H 'flipped' to the other side. At the same time, the torus curve emanating from G_1 now appears on the other side of G_1; see [29] for more details. The main features of Figure 9 (f) are the two regions bounded by what remains of the curve P_0. These two regions have been identified as a parameter region where semiconductor lasers produce chaos; see [29,32]. The routes to chaos differ depending on how the regions are entered, and they include sudden transitions, such as boundary crises and intermittency [31,33,34].

The remainder of the bifurcation structure near G_1 is a cascade of torus bifurcations, as is shown in Figure 10 (a), which also incorporates the remainder of the curve P_0. The pieces of torus curves T^i are connected at 1:1 resonances to saddle-node of limit cycle curves; see Figure 10 (b). The region inside P_0 contains unnested islands of period-doublings that lead to further bifurcations; see [34].

Notice that the *position* of G_1 does not change much throughout the transition we described, even though its type does. (In fact, there are further changes of its type; see [14,24,25].) However, the overall bifurcation structure near G_1 changes dramatically. Nevertheless, two main regions where semiconductor lasers are known to show chaotic dynamics have been identified as 'remainders' associated with the single region bounded by the curve P^0 for $\alpha = 0$. The accumulating regions break up quickly, and this explains that a period-adding cascade has never been found for semiconductor lasers.

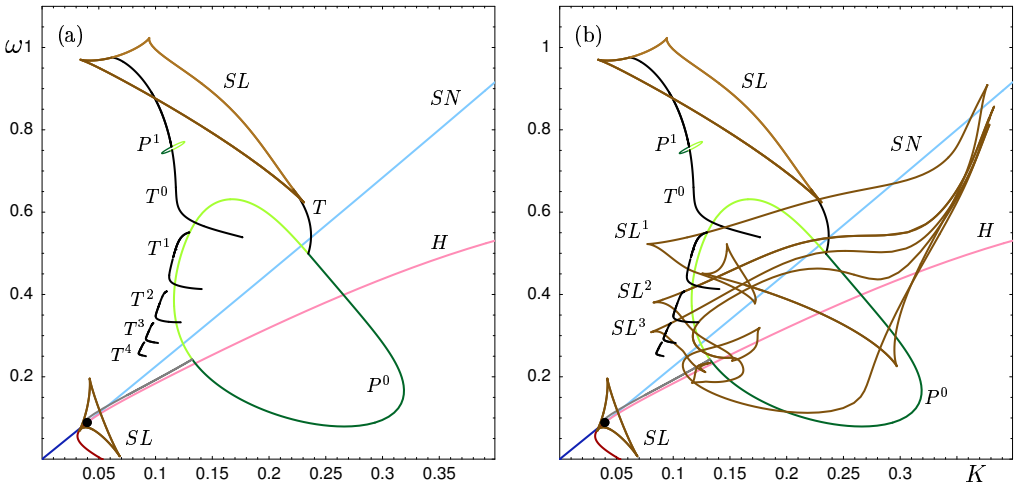

Fig. 10. Cascade of torus bifurcation curves in the (K, ω)-plane for $\alpha = 2.0$; panel (a) shows the main bifurcation curves and panel (b) the structure of further saddle-node of limit cycle curves.

4.2 Negative detuning

It is in the nature of the linewidth enhancement factor α to lead to a different reaction of the laser to input with positive and negative detuning [**?**, p. 287]. This is brought out clearly in Figure 11 where we show the change in accumulating regions of winding periodic orbits for negative detunings as α is increases to values in the range of semiconductor lasers.

Again, for ease of reference Figure 11 (a) shows the accumulating regions for $\alpha = 0$. (Recall that in this case the SN-Hopf point G_2 is the mirror image of G_1.) Also for negative ω these regions disappear quickly, but in a different way. The point G_2 moves rapidly to larger values of K and 'drags' the accumulating regions with it; see Figure 11 (b). As α is increased further, we are left with a number of regions along the torus bifurcation curve T, which is almost parallel to the lower locking boundary SN; see Figure 11 (c). The point G_2 has already disappeared to values of K that are physically hard to realise. We remark that G_2 moves through a cusp of the curve SN (at very large values of K) when α moves through one; see [29] for details. As mentioned before, this also marks the transition to the case of semiconductor lasers, via the 'flip' of the supercritical part of the Hopf curve H, leading to the characteristic shape of the locking region in Figure 11 (d). What remains of the accumulating regions is a bifurcation structure for negative detunings that is typical for semiconductor lasers, with different bifurcations on the route to locking; see [12,30] for details.

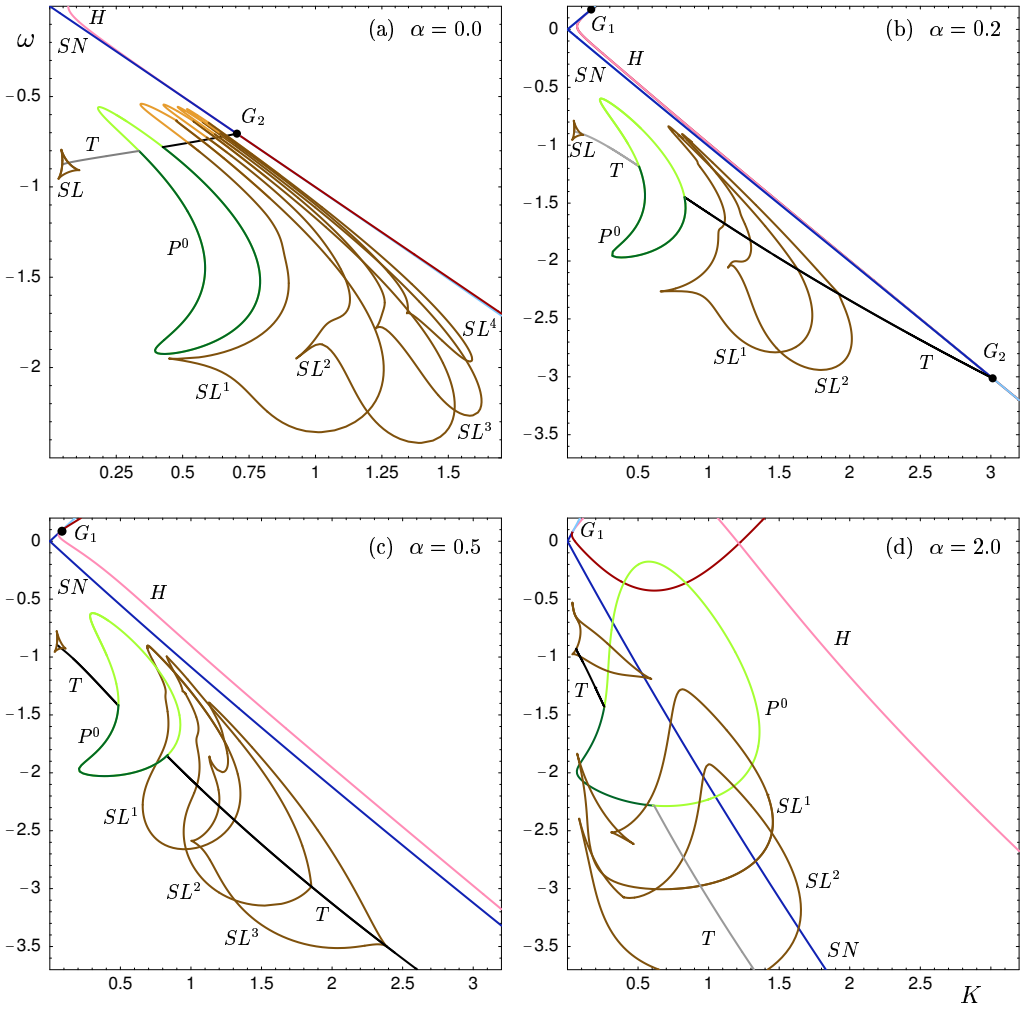

Fig. 11. Transition of the accumulating regions in the (K, ω)-plane for negative detunings ω with increasing α; from (a) to (d) α takes the values 0.0, 0.2, 0.5, and 2.0.

As for positive detunings, we conclude that the accumulating regions disappear quickly, but the bifurcation structure behind it survives in large parts. This gives rise to regions of complicated dynamics and to bifurcations that were identified in semiconductor lasers before. In particular, the torus bifurcation T has been found analytically in [28] by considering the limit of large α. It is responsible for a bistability between the a running phase solution and locking [5,28,30], when T and the subcritical part of SN intersect.

5 Conclusions

The mechanism of a period-adding cascade, observed both in experimental and theoretical investigations of class B lasers with injected signal since the mid 1980's, is due to accumulating regions of winding periodic orbits near a saddle-node-Hopf point with global reinjection. This bifurcation structure is present only for non-chirping lasers, such as solid-state and CO_2 lasers for which α is practically zero, but disappears quickly when α is positive. Nevertheless, the respective bifurcation curves can be followed to values of α in the range typical for semiconductor lasers, providing a link between these different types of lasers. Indeed, certain regions in the bifurcation diagram of semiconductor lasers can be viewed as 'remains' of the accumulating regions for $\alpha = 0$.

Our studies indicate that the bifurcation diagram is organised by the saddle-node-Hopf point, whose important feature is that it occurs on a periodic orbit, which provides a global reinjection mechanism. While the local dynamics near a saddle-node-Hopf point is quite well known, the global reinjection introduces new dynamics. An instance of this are the winding periodic orbits with different numbers of big loops. How they are organised, and how they bifurcate in homoclinic bifurcations, is a topic of ongoing research.

Acknowledgements

We thank Daan Lenstra, Steve Strogatz and Stephen Yeung for helpful discussions, and Steve Coombes for pointing out reference [51] of the period-adding cascade. The research of S.W. was supported by the Foundation for Fundamental Research on Matter (FOM), which is financially supported by the Netherlands Organization for Scientific Research (NWO).

References

[1] S. Kobayashi and T. Kimura, "Injection locking characteristics of an ALGaAs semiconductor laser", *IEEE J. Quantum Electron.* **16** (1980) 915–917.

[2] R. Lang, "Injection locking properties of a semiconductor laser", *IEEE J. Quantum Electron.* **18** (6) (1982) 976–983.

[3] F. Mogensen, H. Olesen and G. Jacobsen, "FM noise suppression and linewidth reduction in an injection-locked semiconductor laser", *Electron. Lett.* **21** (1985) 696–697.

[4] G.L. Oppo, A. Politi, G.L. Lippi and F.T. Arecchi, "Frequency pushing in lasers with injected signal", *Phys. Rev. A* **34** (5) (1986) 4000–4007.

[5] R. Hui, A. D'Ottavi, A. Mecozzi, P. Spano, "Injection locking in distributed feedback semiconductor lasers" *IEEE J. Quantum Electron.* **27** (1991) 1688.

[6] L.A. Lugiato, L.M. Narducci, D.K. Bandy, C.A. Pennise, "Breathing, spiking and chaos in a laser with injected signal", *Opt. Comm.* **46** (1983) 64–68.

[7] F. Mogensen, G. Jacobsen and H. Olesen, "Light intensity pulsations in an injection locked semiconductor laser", *Opt. Quantum Electron.* **16** (1984) 183–186.

[8] P.A. Braza and T. Erneux, "Constant phase, phase drift and phase entrainment in lasers with an injected signal", *Phys. Rev. A* **41** (11) (1990) 6470–6479.

[9] J. Sacher, D. Baums, P. Panknin, W. Elsäßer and E.O. Göbel, "Intensity instabilities of semiconductor lasers under current modulation, external light injection and delayed feedback", *Phys. Rev. A* **45** (3) (1992) 1893–1905.

[10] E.-K. Lee, H.-S. Pang, J.-D. Park and H. Lee, "Bistability and chaos in an injection-locked semiconductor laser", *Phys. Rev. A* **47** (1) (1993) 736–739.

[11] G.H.M. van Tartwijk, G. Muijres, D. Lenstra, M.P. van Exter and J.P. Woerdman, "The semiconductor laser beyond the locking range of optical injection", *Electronics Letters* **29** (1993) 137–138.

[12] D. Lenstra, G.H.M. van Tartwijk, W.A. van der Graaf, and P.C. De Jagher, "Multi-wave mixing dynamics in a diode laser", *Chaos in Optics, Proc. SPIE* **2039** (1993) 11–22.

[13] V. Annovazzi-Lodi, S. Donati and M. Manna, "Chaos and locking in a semiconductor laser due to external injection", *IEEE J. Quantum Electron.* **30** (7) (1994) 1537–1541.

[14] H.G. Solari, G.L. Oppo, "Laser with injected signal: perturbation of an invariant circle", *Opt. Comm.* **111** (1994) 173–190.

[15] T.B. Simpson, J.M. Liu, A. Gavrielides, V. Kovanis and P.M. Alsing, "Period-doubling route to chaos in a semiconductor laser subject to optical injection", *Appl. Phys. Lett.* **64** (26) (1994) 3539–3541.

[16] T.B. Simpson, J.M. Liu, A. Gavrielides, V. Kovanis and P. M. Alsing, "Period-doubling cascade and chaos in a semiconductor lasers with optical injection", *Phys. Rev. A* **51** (5) (1995) 4181–4185.

[17] V. Kovanis, A. Gavrielides, T.B. Simpson, J.M. Liu, "Instabilities and chaos in optically injected semiconductor lasers", *Appl. Phys. Lett.* **67** (19) (1995) 2780–2782.

[18] P.C. de Jagher, W.A. van der Graaf, D. Lenstra, "Relaxation-oscillation phenomena in an injection locked semiconductor laser", *Quant. Semiclass. Opt.* **8** (1996) 805–822.

[19] T. Erneux, V. Kovanis, A. Gavrielides and P.M. Alsing, "Mechanism for period-doubling bifurcation in a semiconductor laser subject to optical injection", *Phys. Rev. A* **53** (6) (1996) 4372–4380.

[20] T. Erneux, A. Gavrielides and V. Kovanis, "Low pump stability of an optically injected diode laser", *Quant. Semiclass. Opt.* **9** (5) (1997) 811–818.

[21] A. Gavrielides, V. Kovanis, P.M. Varangis, T. Erneux and G. Lythe, "Coexisting periodic attractors in injection-locked diode lasers" *Quant. Semiclass. Opt.* **9** (5) (1997) 785–796.

[22] T.B. Simpson, J.M. Liu, K.F. Huang and K. Tai, "Nonlinear dynamics induced by external optical injection in semiconductor lasers", *Quant. Semiclass. Opt.* **9** (5) (1997) 765–784.

[23] M.G. Zimmermann, M.A. Natiello and H. Solari, "Shilnikov-Saddel-node interaction near a codimension 2 bifurcation: laser with injected signal", *Physica D* **109** (3-4) (1997) 293–314.

[24] B. Krauskopf, W.A. van der Graaf and D. Lenstra, "Bifurcations of relaxation oscillations in an optically injected diode laser", *Quant. Semiclass. Opt.* **9** (1997) 797–809.

[25] B. Krauskopf, N. Tollenaar and D. Lenstra, "Tori and their bifurcations in an optically injected semiconductor laser", *Opt. Comm.* **156** (1998) 158–169.

[26] M.K.S. Yeung and S.H. Strogatz, "Nonlinear dynamics of a solid-state laser with injection", *Phys. Rev. E* **58** (4) (1998) 4421–4435; Erratum, *Phys. Rev. E* **61** (2) (2000) 2154.

[27] V. Kovanis, T. Erneux and A. Gavrielides, "Largely detuned injection-locked semiconductor lasers", *Opt. Comm.* **159** (1999) 177–183.

[28] M. Nizette, T.Erneux, A. Gavrielides, and V. Kovanis, "Injection locked semiconductor laser dynamics from large to small detunings", *Proc. SPIE* **3625** (1999) 679–689

[29] S. Wieczorek, B. Krauskopf and D. Lenstra, "A unifying view of bifurcations in a semiconductor laser subject to optical injection", *Opt. Comm.* **172**(1-6) (1999) 279-295.

[30] S. Wieczorek, B. Krauskopf and D. Lenstra, "Mechanisms for multistability in a semiconductor laser with optical injection", *Opt. Comm.* **183**(1-4) (2000), 215–226.

[31] B. Krauskopf, S.M. Wieczorek and D. Lenstra, "Different types of chaos in an optically injected semiconductor laser", *Appl. Phys. Lett.* **77**(11) (2000), 1611–1613.

[32] S.K. Hwang, and J.M. Liu "Dynamical Characteristics of an optically injected semiconductor laser", *Opt. Comm.* **183** (2000) 195.

[33] S. Wieczorek, B. Krauskopf and D. Lenstra, "Sudden chaotic transitions in an optically injected semiconductor laser", *Opt. Lett.* **26**(11) (2001), 816-818.

[34] S. Wieczorek, B. Krauskopf and D. Lenstra, "Unneseted islands of period-doublings in an injected semiconductor laser", *Phys. Rev. E* **64** 056204 (2001) 1-9.

[35] S. Eriksson and A.M. Lindberg, "Periodic oscillations within the chaotic region in a semiconductor laser subject to optical injection", *Opt. Lett.* **26**(3) (2001) 142–144.

[36] C. Mayol, M.A. Natiello and M.G. Zimmermann, "Resonance structure in a weakly detuned laser with injected signal", *Int. J. Bif. Chaos*, to appear.

[37] S. Wieczorek, T.B. Simpson, B. Krauskopf and D. Lenstra, "Global quantative predictions of complex laser dynamics", preprint.

[38] M. Nizette, T. Erneux, A. Gavrielides, and V. Kovanis, "Averaged equations for injection locked semiconductor lasers", preprint.

[39] M.G. Zimmermann, M.A. Natiello and H. Solari, "Global bifurcations in a laser with injected signal: beyond Adler's approximation", preprint.

[40] G.H.M. van Tartwijk and D. Lenstra, "Semiconductor lasers with optical injection and feedback", *Quant. Semiclass. Opt.* **7** (1995) 87–143.

[41] G.H.M. van Tartwijk and G.P. Agrawal, "Laser instabilities: a modern perspective", *Progr. Quant. Electron.* **22** (1998) 43

[42] B. Krauskopf and D. Lenstra (Eds.), *Fundamental Issues of Nonlinear Laser Dynamics*, AIP Conference Proceedings **548** (2000)

[43] H.F. Chen and J.M. Liu, "Open Loop Chaotic Synchronization of Injection Locked Semiconductor Lasers with Gigahertz Range Modulation", *IEEE. J. of Quatum Electron.* **36** (2000) 27–34.

[44] G. P. Agrawal and N. K. Dutta, *Semiconductor Lasers, second edition*, Van Nostrand, New York (1993).

[45] J. Guckenheimer and P. Holmes, *Nonlinear Oscillations, Dynamical Systems and Bifurcations of Vector Fields*, Second Printing, Springer 1986.

[46] Yu.A. Kuznetsov, *Elements of Applied Bifurcation Theory*, Applied Mathematical Sciences **112**, Springer 1995.

[47] K.S. Thornburg, Jr., M. Möller, R. Roy, T.W. Carr, R.-D. Li, and T. Erneux, "Chaos and coherence in coupled lasers", *Phys. Rev. E* **55** (1997) 3865–3869.

[48] E. Brun, B. Derighetti, D. Meier, R. Holzner and M. Ravani, "Observation of order and chaos in a nuclear spin-flip laser", *J. Opt. Soc. Am. B* **2**(1) (1985) 156–167.

[49] J.R. Tredicce, F.T. Arecchi, G.L. Lippi and G.P. Puccioni, "Instabilities in lasers with an injected signal", *J. Opt. Soc. Am. B* **2** (1) (1985) 173–183.

[50] J. L. Boulnois, A van Lerberghe, P. Cottin, F. T. Arecchi, and G. P. Puccioni, "Self pulsing in a CO_2 ring laser with an injected signal." *Opt. Comm.* (58) (1986) 124–129.

[51] W. Lauterborn and I. Eick, "Numerical investigation of a periodically driven laser with an intracavity saturable absorber", *J. Opt Soc. Am. B* **5**(5), 1089–1096.

[52] M. Sargent III, M. O. Scully, and W. E. Lamb Jr., *Laser Physics*, Addison-Wesley Publ. Comp., Reading Mass. (1974).

[53] F. T. Arecchi, G. Lippi, G. Puccioni, and J. Tredicce, in "Coherence in Quantum Optics V", L. Mandel and E. Wolf, eds., p. 1227, Plenum, New York (1984).

[54] E. Doedel, T. Fairgrieve, B. Sandstede, A. Champneys, Yu. Kuznetsov and X. Wang, "AUTO 97: Continuation and bifurcation software for ordinary differential equations", *http://indy.cs.concordia.ca/auto/main.html*

[55] A. Back, J. Guckenheimer, M.R. Myers, F.J. Wicklin and P.A. Worfolk, "DsTool: Computer assisted exploration of dynamical systems", *Notices Amer. Math. Soc.* **39** (1992) 303-309.

[56] B. Krauskopf and H.M. Osinga, "Growing 1D and quasi 2D unstable manifolds of maps" *J. Comp. Phys.* **146**(1), 404 (1998);

[57] B. Krauskopf and H.M. Osinga, "Investigating torus bifurcations in the forced Van der Pol oscillator", in E.J. Doedel and L.S. Tuckerman (Eds.), *Numerical Methods for Bifurcation Problems and Large-Scale Dynamical Systems*, IMA Volumes in Mathematics and its Applications **119**, Springer-Verlag (2000) pp 199–208.